Available online at www.sciencedirect.com
SCIENCE DIRECT
ELSEVIER
European Journal of Mechanics B/Fluids 23 (2004) 861–878
EUROPEAN JOURNAL OF MECHANICS B/FLUIDS

Nonlinear effects on edge wave development

Veronica Galletta, Giovanna Vittori *

Department of Environmental Engineering, University of Genova, via Montallegro 1, 16145 Genova, Italy

Received 14 January 2004; received in revised form 29 April 2004; accepted 4 May 2004

Available online 29 July 2004

Abstract

The effect of nonlinearity on the evolution of free edge waves is investigated by solving numerically the nonlinear shallow water equations. The numerical scheme is the two-dimensional WAF method, originally developed by Toro [Riemann Solvers and Numerical Methods for Fluid Dynamics, Springer, 1997]. First, a simple beach geometry [J. Fluid Mech. 381 (1999) 271] is considered and the numerical results are validated against available analytical solutions for small amplitude edge waves. Then, results are obtained for edge waves of larger amplitude. Nonlinear effects are found to be relevant even for moderate values of the nonlinearity parameter a which is the ratio between the wave amplitude and the water depth. In particular a resonance phenomenon has been observed which causes a modulation in time of the ultra-harmonic components of the wavefield. Larger values of a lead to a complex time evolution.

1. Introduction

The existence of edge waves in nature has been known for a long time. Field measurements show that low frequency edge waves can form a significant portion of the energy spectrum in the nearshore region, especially when the bottom morphology is characterized by the presence of 3-D morphological patterns like cusps, welded bars, crescentic forms [1,2].

As discussed in Mei [3], different mechanisms for edge wave generation on sloping beaches are possible.

Small-scale edge waves can be generated by short wind waves through a subharmonic resonance mechanism as discussed by Guza and Davis [4], Guza and Bowen [5] and Minzoni and Whitham [6]. Medium-scale edge waves can be excited by a long group of short swells approaching a beach through a nonlinear mechanism. Long edge waves can be excited by external forcings such as wind stresses or uneven pressure distributions related to storms traveling parallel to the coast. Moreover, tsunami generated by an earthquake near the coastline can be trapped by the continental shelf and energetic coastal edge waves are thus generated [7]. As a consequence the characteristic period of edge waves observed in the field ranges from seconds to hours.

Several authors have suggested that edge waves may play an important role in many phenomena characterizing both the hydrodynamics and the morphodynamics of the nearshore region. Bowen [8] and Bowen and Inman [9] discussed a mechanism by which edge waves could control the longshore spacing of rip currents. Inman and Guza [10] showed that the interaction between an incident monochromatic wave and edge waves produces a longshore periodic pattern in the swash water motion which, in turn, is supposed to modify the morphology of the beach face. Also the periodic morphological features which are located outside the breaker zone are often related to the presence of edge waves. For example, Holman and Bowen [11] showed that the steady drift, generated by the nonlinear self interaction of edge waves inside the bottom boundary layer, can cause a net displacement of the sediment and give rise to bottom patterns similar to those detected in the field. The trapping of edge waves

* Corresponding author. Fax: +39-010-353-2546.
E-mail address: vittori@diam.unige.it (G. Vittori).

0997-7546/$ – see front matter
doi:10.1016/j.euromechflu.2004.05.002

on nearshore waveguides, such as bars and longshore currents, has been presented as a possible mechanism for the growth and movement of longshore bars [12–14]. More recently Vittori et al. [15] have shown that a wave approaching the coast and interacting with small bottom perturbations can produce synchronous edge waves. These edge waves subsequently interact with the incoming wave and generate steady currents. This steady streaming induces a net sediment transport with a convergence pattern that, depending on the geometry of the beach and on wave characteristics, may be in phase with the initial bedforms. Hence, there may be a positive feedback between the water motion and the erodible bottom which gives rise to a mechanism able to trigger the appearance of alongshore periodic crescentic bedforms.

Analytical solutions for edge waves exist only for particular types of beach profile. Eckart [16] solved the shallow water equations for a plane beach, while Ball [17] tackled the problem for a beach profile such that the water depth exponentially tends to a constant value. While Eckart's profile is appropriate to study edge waves in the surf region, Ball's profile has been proposed to describe phenomena that involve waves that are trapped between the continental shelf and the deep-sea region where the water depth can be assumed to be constant [7]. In Blondeaux et al. [18] an extension of Eckart's solution is described where a constant sloping beach delimited by a vertical wall is considered. The model beach introduced by Blondeaux et al. [18] and later used by Vittori et al. [15] is particularly effective when attention is focused on medium scale edge waves characterized by periods of the order of minutes, i.e. on water motions confined in the continental shelf but with a horizontal extent larger than the surf region width. Indeed, when water motions characterized by a length scale larger than the surf region width are considered, a comparison of actual sea bottom topographies with the beach profile proposed by Blondeaux et al. [18] (see the second and third paragraphs) shows that the latter provides an approximation better than that obtained by means of Eckart's [16] profile.

All the investigations mentioned above are based on the linearized shallow water equations. The assumption of water depths much smaller than the horizontal length scale of edge waves is well justified in the field. Indeed, even for the short edge waves which are present in the surf region, the water depth is at least one order of magnitude smaller than the wavelength. However on the basis of the results described in the following it can be inferred that the assumption of small amplitudes, which makes nonlinear effects negligible, is not always appropriate.

Indeed, the present results suggest that the edge wave behavior departs from the linear regime as the nonlinearity parameter $a = a^*/h_0^*$ (a^* is the amplitude of the edge wave and h_0^* the reference depth) assumes values of order 10^{-2}. In particular, when a attains values of order 10^{-2}, nonlinear effects induce an energy transfer among the different components of the edge wave spectrum and a resonance phenomenon may take place. This resonance mechanism, presently studied by means of both a weakly nonlinear analysis and a numerical approach, leads to modulations of the edge wave amplitude taking place on a long time scale. These resonance effects should be relevant in the dynamics of the infra-gravity edge waves observed in the field since existing data (a.o. [19]) suggest that the total edge wave frequency band has shoreline amplitudes of the order of ten centimeters. While observations on open coastal beaches [19,20] show the existence of a broad-banded edge-wave field, measurements on a narrow pocket beach [20] show that only a limited number of edge waves frequencies is present and that a single edge wave attains amplitudes of the order of a few centimeters. Such values of the edge wave amplitude, combined with water depths of the order of meters, give rise to values of the parameter a of order 10^{-2}.

Moreover, the analysis of Guza and Bowen [21] shows that the amplitude of edge waves generated by 2-D waves approaching the nearshore region from the deep sea, depends on the amplitude of the incoming wavefield. Then, it is likely that field conditions more severe than those observed by Oltman-Shay and Guza [19] and Őzkan-Haller et al. [20] generate edge waves of larger amplitudes and give rise to values of the parameter a larger than 10^{-2}. In such cases the present results show that numerical approaches are needed to describe the nonlinear effects which affect edge wave dynamics and give rise to complex interactions between different edge wave modes.

Strong nonlinear effects are also relevant when studying the dynamics of edge waves associated to tsunami propagation along sloping coasts. In fact the observations of Gonzales et al. [22] suggest that edge waves of large amplitude could be generated by relatively small earthquakes because of the resonant interactions of the tsunami wave with the bottom topography. Indeed Gonzales et al. [22], far from the region of tsunami generation, observed edge wave amplitudes larger than those measured close to the generation area.

The aim of the present paper is to investigate the role of nonlinear effects in the evolution of medium scale edge waves. Because the presence of strong nonlinearities prevents the use of analytical means, in the present work the numerical simulation of the fully nonlinear shallow water equations is carried out. Attention is focused on the model beach suggested by Blondeaux et al. [18] since it is the most appropriate to investigate medium scale edge waves. Moreover, a solution of the linearized problem in analytical form is available and hence it is straightforward to estimate the relevance of nonlinear effects by comparing the numerical results with the linear analytical findings. The numerical approach is based on the weighted average flux method (WAF) originally developed by Toro [23]. The WAF method is a 'shock capturing' numerical scheme which is particularly effective when studying hydrodynamic phenomena with strong nonlinearities. Unidimensional versions of this numerical scheme have been successfully applied to describe wave breaking and run-up on a sloping beach [24]. Presently a two-dimensional version of the method is applied which is similar to that described in Brocchini and Vittori [25] and Brocchini

et al. [26]. The dynamics of edge waves for small but finite amplitudes is investigated also by means of a weakly nonlinear approach. In literature (see a.o. Mei [3]) weakly nonlinear approaches are used to describe the interaction of an incoming wavefield with subharmonic edge waves. Guza and Bowen [5] studied the phenomenon on a planar beach obtaining the time evolution of the amplitude of edge waves till equilibrium is attained, the set-down and the energy radiation toward the deep sea region related to the presence of edge waves. More recently, Blondeaux and Vittori [27] have taken into account the interaction between an incoming wavefield and edge waves of different frequencies showing the existence of a mechanism able to trigger the formation of edge wave which are synchronous with respect to the frequency of the incoming wave. A weakly nonlinear analysis has been applied by Kirby et al. [28] to investigate the triadic resonances between coastally-trapped gravity and vorticity waves for a planar beach. Indeed, even though the possibility of triadic interactions among progressive edge waves was already mentioned in literature [29], no calculations were provided. The results of Kirby et al. [28], who considered explicitly only cases characterized by the absence of the longshore current and presented results for cases where shear waves are absent, allow the time development of the edge wave amplitudes to be quantified. In particular Kirby et al. [28] show that, for triads of edge waves involving counter-propagating waves, the interactions are fairly rapid while the triads involving only edge waves propagating in the same direction did not show any interaction. However, as pointed out by Kirby et al. [28] themselves, the limitation of their theory to the cases of waves on a planar beach topography is restrictive, particularly for medium and large scale edge waves and their work needs to be extended to the case of non-planar topographies.

Presently, a weakly nonlinear approach is used to describe the interactions of different edge wave components on the model beach introduced by Blondeaux et al. [18]. The case studied in detail is that of a standing edge wave of frequency σ and wavenumber k_1 resonantly interacting with another standing edge wave characterized by a frequency equal to $2\sigma_1 + \mu$ and by a wavenumber equal to $2k_1$, where μ is a small mismatch parameter. This resonance cannot occur on a plane beach (e.g. Kirby et al. [28]) and this further supports the need to investigate more complex beach topographies. Although the numerical code, by using appropriate initial and boundary conditions, could describe the weakly nonlinear triadic interactions investigated by Kirby et al. [28], in the following such interactions will not be considered and attention will be focused only on standing edge waves. Present results show the existence of modulations of the edge wave amplitudes which take place on a time scale much longer than the period of edge waves and fairly compare with the numerical results.

It is important to point out that the analysis by Blondeaux and Vittori [27], as well as previous weakly nonlinear approaches, are unable to provide the bounds of validity of the analyses themselves. In this respect the fully nonlinear approach adopted here can be used also to detect when the nonlinear effects become strong and cannot be described by a weakly nonlinear analysis.

The procedure used in the rest of the paper is as follows. In the next section the problem is formulated and a brief description of the numerical approach is given. In the third section the results are described.

Results are presented for moderate as well as large wave amplitudes such that nonlinear effects are weak and strong respectively. As previously pointed out, in the weakly nonlinear regime, due to the interaction of different edge waves, the obtained results show a modulation of the edge wave amplitudes. Since this finding has never been reported in literature, to support this numerical finding, a weakly nonlinear analysis, described in the third section, is developed. The agreement between the theoretical results and the numerical ones provide further validation for the numerical code. The last section is devoted to the conclusions and to the description of the possible developments of the work.

2. Formulation of the problem

Fig. 1 shows a sequence of beach profiles observed during field measurements carried out at the coast of Duck (North Carolina) [30,31]. From Fig. 1 it can be appreciated that the region closest to the shore, of the order of 100 meters, is characterized by a large slope which decreases moving in the offshore direction and becomes almost constant in the region further offshore. As discussed in Vittori et al. [15], when wave motions of large wavelengths are considered, a model beach with a constant slope cannot be assumed to describe field topographies, unless it is delimited by a vertical wall located somewhere in the surf region (see Fig. 1). If this geometry is considered, the water depth in still water conditions is described by

$$h^* = h_0^* + \beta x^*. \tag{1}$$

In (1) x^* is the cross-shore coordinate such that $x^* = 0$ is the location of the wall and β is the bottom slope in the offshore region (see Fig. 2). Of course the use of (1) implies that the swash and surf regions do not play a significant role in the dynamics of the large scale motions. Moreover, transient phenomena of small scale, like storm-generated longshore bars, are neglected. The two independent parameters (h_0^* and β) characterizing the model beach can be determined by fitting the observed field profiles. For example, for the beach profiles shown in Fig. 1, it turns out that the optimized values of h_0^* and β are equal to 2.65 m and 0.7×10^{-2} respectively, even though an analysis of the beach profiles at different locations can give rise to different values. For example the data of Niigata and Tokai beaches [32] suggest values of h_0 close to 2.5 m and values of β ranging around 0.8×10^{-3} and the data of Lubiatowa beach [33] provide values for h_0 close to 2.1 m and β ranging around 6×10^{-3}.

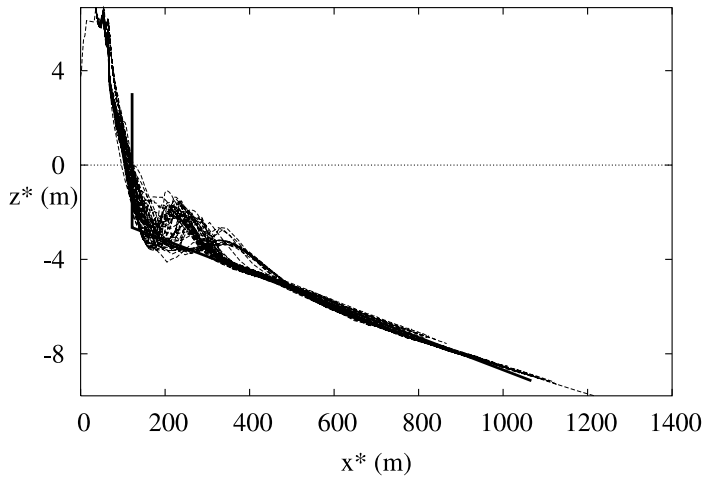

Fig. 1. Some of the beach profiles observed at Duck (North Carolina) by Howd and Birkemeijer [30] and Lee and Birkemeijer [31] along with the optimized beach geometry (h_0=2.65 m, $\beta = 0.7 \times 10^{-2}$).

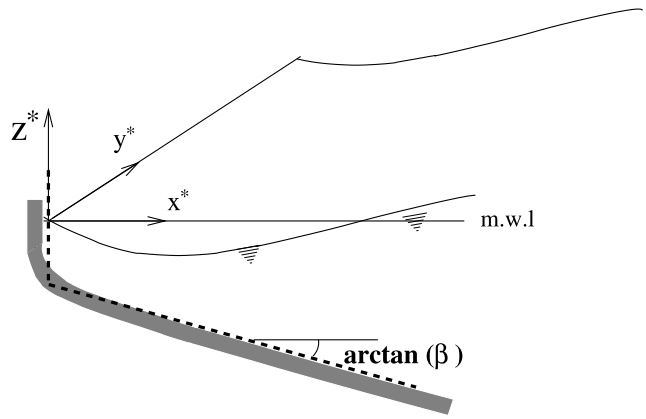

Fig. 2. Sketch of the problem.

Since attention is focused on edge waves of wavelength much larger than the surf region width, the model beach (1) is adopted in the computations.

The comparison, shown in Fig. 3, between the first free edge wave mode on the model beach (1) [18] and that described in Eckart [16] for a constant sloping beach shows that no significant differences are present in the cross-shore edge wave profile. The comparison has been performed considering beaches characterized by the same slope β ($\beta = 0.01$) and edge waves with the same longshore wavenumber ($k^* = 2\pi/L_y^* = 1.29 \times 10^{-2}$ m^{-1}). Moreover the vertical wall of the beach profile (1) is located at a cross section such that $h_0^* = 2$ m. However significant differences are found in the dispersion relationship. Indeed for the selected wavenumber, the ratio between the frequency of the edge wave on the plane beach and that characterizing the edge wave on the beach profile described by (1) is equal to about 1.9.

Here the shallow water equations are considered in dimensionless form. By denoting with ω^* the angular frequency of the dominant edge wave mode computed on the basis of the linear dispersion relationship described in the following (see Section 3) and with g^* the gravitational acceleration, the horizontal lengths are scaled with $\sqrt{g^* h_0^*}/\omega^*$, while the water depth h^* and the free surface elevation η^* are scaled with h_0^*. Moreover the velocities are scaled with $\sqrt{g^* h_0^*}$ and the time with $(\omega^*)^{-1}$. It can be easily verified that in the dimensionless problem the beach geometry is identified by the dimensionless parameter $x_w = \omega^* \sqrt{h_0^*}/(\beta\sqrt{g^*})$. Dropping the '*' to indicate dimensionless quantities, the conservative form of the governing equations becomes:

$$\mathbf{U}_t + \mathbf{F}_x + \mathbf{G}_y = \mathbf{S}(\mathbf{U}), \tag{2}$$

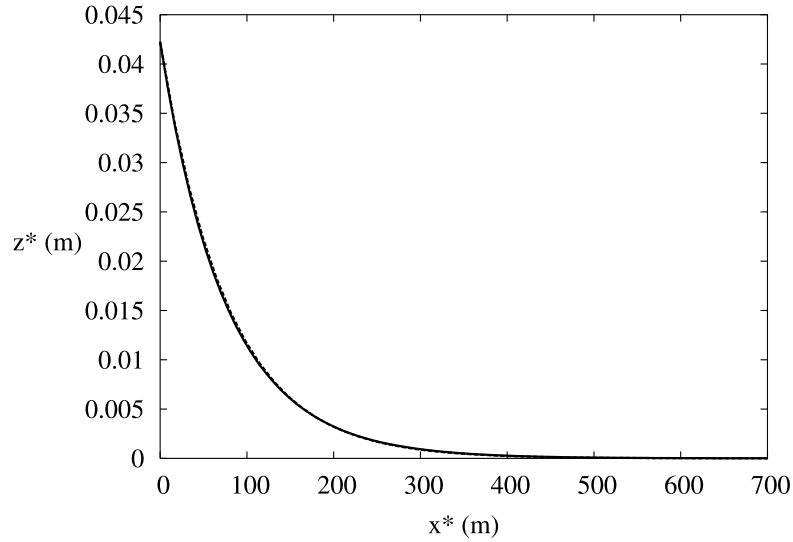

Fig. 3. Amplitude of the first free edge wave mode: — beach profile (1) ($T^* \approx 95$ s); - - - beach profile with constant slope without a vertical wall ($T^* \approx 177$ s). ($k^* = 1.29 \times 10^{-2}$ m^{-1}, $\beta = 0.01$, $h_0^* = 2$ m).

where $\mathbf{U} = (\phi, \phi u, \phi v)$ is the vector of the unknowns related to the conserved quantities mass and momentum, $\mathbf{F} = (\phi u, \phi u^2 + \frac{1}{2}\phi^2, \phi uv)$ and $\mathbf{G} = (\phi v, \phi uv, \phi v^2 + \frac{1}{2}\phi^2)$ are the fluxes of these quantities and $\mathbf{S} = (0, \phi h_x, \phi h_y)$ is the source term due to the beach slope. In the previous definitions ϕ is equal to $h + \eta$, where h and η are the dimensionless water depth and free surface elevation respectively and u and v denote depth-averaged cross-shore and long-shore velocity components respectively. Moreover t, x, y indicate time, cross-shore and long-shore coordinates respectively and a subindex denotes partial derivative (see Fig. 2).

The numerical scheme presently used to determine the solution of (2) is a high resolution conservative method based on the solution of local Riemann problems. The method has been originally developed by Toro [23] and it is known under the name of 'weighted average flux method' (WAF). Comparisons performed with the Lax–Wendroff scheme have shown that the WAF method is particularly efficient and requires a smaller number of collocation points to provide accurate results [34]. Moreover the adopted numerical scheme is particularly effective in reproducing the steepening of the waves and the formation of discontinuities (bores) without the need for a special tracking algorithm.

Presently a two-dimensional version of the method is applied. In the following only the main aspects of the method will be described. For details the reader is referred to Toro [23,35], Watson et al. [36] and Galletta [34]. First, following Watson et al. [36], the problem is reformulated to incorporate the source term $\mathbf{S}(\mathbf{U})$ into the flux terms ($\mathbf{F}$ and $\mathbf{G}$). This is obtained by observing that the set of Eqs. (2) in the accelerating reference frame

$$\zeta = x - \frac{1}{2}gh_x t^2, \qquad \chi = y - \frac{1}{2}gh_y t^2, \qquad \tau = t \tag{3}$$

becomes

$$\begin{pmatrix} \hat{\phi} \\ \hat{\phi}\hat{u} \\ \hat{\phi}\hat{v} \end{pmatrix}_\tau + \begin{pmatrix} \hat{\phi}\hat{u} \\ \hat{\phi}\hat{u}^2 + \frac{1}{2}\hat{\phi}^2 g \\ \hat{\phi}\hat{u}\hat{v} \end{pmatrix}_\zeta + \begin{pmatrix} \hat{\phi}\hat{v} \\ \hat{\phi}\hat{u}\hat{v} \\ \hat{\phi}\hat{v}^2 + \frac{1}{2}\hat{\phi}^2 g \end{pmatrix}_\chi = \begin{pmatrix} 0 \\ 0 \\ 0 \end{pmatrix} \tag{4}$$

or with a compact notation

$$\widehat{\mathbf{U}}_\tau + \widehat{\mathbf{F}}_\zeta + \widehat{\mathbf{G}}_\chi = 0, \tag{5}$$

where

$$\hat{\phi} = \phi, \qquad \hat{u} = u - gh_x t, \qquad \hat{v} = v - gh_y t. \tag{6}$$

Then, from the knowledge of the solution $\widehat{\mathbf{U}}_{ij}^n$ at time $t^n = n\Delta t$ and in the point (ζ_i, χ_j) ($\zeta_i = i\Delta\zeta$, $\chi_j = j\Delta\chi$), the value of $\widehat{\mathbf{U}}_{ij}^{n+1}$ is obtained using a space-operator splitting [35], whereby the two-dimensional problem is reduced to a sequence of

one-dimensional problems. This is achieved by performing first an ζ-sweep thus obtaining an intermediate solution $\widetilde{\mathbf{U}}_{ij}$ and subsequently a χ-sweep [23]. At each sweep the WAF method is applied to the one-dimensional problem

$$\widetilde{\mathbf{U}}_{i,j} = \widehat{\mathbf{U}}^{n}_{i,j} + \frac{\Delta t}{\Delta \zeta}\big[\widehat{\mathbf{F}}^{n+1/2}_{i-1/2,j} - \widehat{\mathbf{F}}^{n+1/2}_{i+1/2,j}\big], \tag{7}$$

$$\widehat{\mathbf{U}}^{n+1}_{i,j} = \widetilde{\mathbf{U}}_{i,j} + \frac{\Delta t}{\Delta \chi}\big[\widehat{\mathbf{G}}^{n+1/2}_{i,j-1/2} - \widehat{\mathbf{G}}^{n+1/2}_{i,j+1/2}\big]. \tag{8}$$

The intermediate fluxes at each cell midpoint $\widehat{\mathbf{F}}^{n+1/2}_{i-1/2,j}$, $\widehat{\mathbf{F}}^{n+1/2}_{i+1/2,j}$, $\widehat{\mathbf{G}}^{n+1/2}_{i,j+1/2}$ and $\widehat{\mathbf{G}}^{n+1/2}_{i,j-1/2}$ are estimated on the basis of the solution of an initial value Riemann problem by means of the approximate 'two rarefaction solver'. For the sake of brevity the explicit relationships providing the fluxes are not given. The interested reader can find details in Toro [35], where an exhaustive description of the approach is also given. To eliminate spurious oscillations, an adjustment is made to the fluxes, using an approach known as Total Variation Diminishing (TVD) with the flux limiter SUPERAA [35] to reweight the average.

The inclusion of the source term **S** into the flux terms (**F** and **G**) is made to avoid first order errors commonly encountered when using simple time-operator splitting in the treatment of the source term **S**(**U**). The numerical approach is thus characterized by errors of order $(\Delta\zeta)^2$, $(\Delta\chi)^2$. The equations are solved in a domain the width of which is L_y in the longshore direction and which extends from $x = 0$ to a cross-shore section located L_x far away in the seaward direction. Periodicity is enforced in the longshore direction. By changing the initial conditions, this boundary condition allows to describe both propagating and standing edge waves. At the offshore boundary ($x = L_x$), a transmissive boundary condition is applied which acts as a "transparent" boundary which allows waves to pass through (see Toro [37]). This is implemented introducing two "fictitious" points at $i = M + 1, M + 2$ (M is the number of grid points in the x-direction) and forcing

$$(\hat{\phi}, \hat{u}, \hat{v})_{M+1} = (\hat{\phi}, \hat{u}, \hat{v})_{M},$$
$$(\hat{\phi}, \hat{u}, \hat{v})_{M+2} = (\hat{\phi}, \hat{u}, \hat{v})_{M-1}.$$

At $x = 0$, a reflective boundary condition, which forces the normal velocity to vanish, is applied. The implementation of the reflective boundary condition requires the introduction of two fictitious points at $i = 0, -1$ where it is forced:

$$(\hat{\phi}, \hat{u}, \hat{v})_{0} = (\hat{\phi}, -\hat{u}, \hat{v})_{1},$$
$$(\hat{\phi}, \hat{u}, \hat{v})_{-1} = (\hat{\phi}, -\hat{u}, \hat{v})_{2}.$$

3. Discussion of the results

A first set of results has been obtained in dimensionless form considering the model beach (1) characterized by $x_w = 11.58$, a value of the parameter x_w which has been chosen on the basis of the analysis of many field data sets and by considering edge wave periods of the order of minutes. At the beginning of the numerical simulation, a surface elevation periodic in the long-shore direction has been introduced. Blondeaux et al. [18] showed that, if one standing edge wave of small amplitude is considered, the free surface profile is described by

$$\eta(x, y, t) = A\,\mathrm{e}^{-k(x_w+x)}U\big(d, 1, 2k(x + x_w)\big)\,\mathrm{e}^{\mathrm{i}(ky+\omega t)} + \text{c.c.}, \tag{9}$$

where A is related to the amplitude of the edge wave. The longshore wavenumber k is obtained, once x_w and ω are fixed, by the eigenrelationship

$$U(d, 1, 2kx_w) + 2dU(d + 1, 2, 2kx_w) = 0 \tag{10}$$

with

$$d = \frac{1}{2} - \frac{\omega^2 x_w}{2k}.$$

In (9) and (10) U is the Kummer function [38]. Eq. (10) is satisfied by more than one couple (k, ω). Therefore, more edge wave modes are possible for a specified value of x_w. In the following, for a given value of ω, k denotes the value of the wavenumber of the edge wave mode characterized by the largest wavelength. It is worth pointing out that, because of the chosen time scale, the dimensionless frequency of the first (dominant) mode turns out to be equal to one (i.e. $\omega = 1$).

The initial edge wave has been chosen to be the first mode and its dimensionless longshore wavelength L_y is fixed by the dispersion relationship (10). For $x_w = 11.58$, L_y turns out to be equal to 6.97. Also the cross-shore decay of the initial surface elevation has been fixed by means of the analytical solution by Blondeaux et al. [18]. Since standing edge waves are often

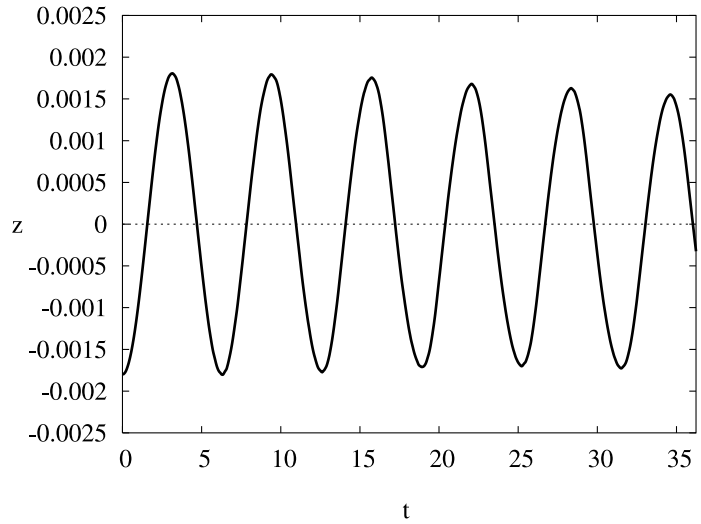

Fig. 4. Time evolution of the free surface displacement at $x = 0.31$ and $y = 3.49$ for an initial perturbation characterized by $L_y = 6.97$, $a = 1.8 \times 10^{-3}$ ($x_w = 11.58$).

observed both on pocket beaches and on infinitely long straight coasts, in the numerical simulations the initial velocity field is forced to be zero. The forcing of an initial nonvanishing flow field would have produced propagating edge waves [18,15].

The computational domain has been chosen with a longshore size equal to the edge wave wavelength. As already pointed out, periodic boundary conditions are forced in the y-direction. At $x = 0$ the cross-shore velocity u is forced to vanish (reflective boundary condition). Moreover in the cross-shore direction, the size L_x of the computational box has been chosen in such a way that no significant motion is present at the seaward boundary ($L_x = 15.44$) and the boundary condition applied there does not affect the solution. The number of grid points has been fixed on the basis of a series of preliminary runs to ensure the accuracy of the results. In particular 2000 and 129 grid points have been used in the cross-shore and long-shore directions respectively. The size of the numerical time step has been varied, while computing the solution, by fixing the maximum value of the Courant number equal to 0.8.

To gain a deeper understanding on the effects of nonlinear terms on edge wave time evolution, the flow field provided by the numerical simulation has been decomposed into Fourier harmonic components in the longshore direction by means of the FFT algorithm:

$$(\eta, u, v) = \sum_{n=-\infty}^{+\infty} \left(\eta^{(n)}(x,t), u^{(n)}(x,t), v^{(n)}(x,t)\right) \mathrm{e}^{\mathrm{i}n(2\pi/L_y)y}. \tag{11}$$

In (11) $\eta^{(0)}$, $u^{(0)}$ and $v^{(0)}$ describe the values of the free surface elevation and of the two velocity components averaged in the longshore direction, while $\eta^{(1)}$, $u^{(1)}$ and $v^{(1)}$ describe the harmonics characterized by the same longshore wavelength as the initial perturbation. The reader should note that, because of the initial conditions, in the present simulations $\eta^{(n)}$, $u^{(n)}$, $v^{(n)}$ turn out to have a vanishing imaginary part.

The analytical solution of the linearized problem for edge waves on the model beach (1) allows a comparison between the numerical simulations and the theoretical results when nonlinear effects are small, i.e. for small (strictly "infinitesimal") values of the parameter a, which gives a measure of the relevance of nonlinear effects. This comparison allows both a validation of the numerical code and an evaluation of the range of validity of the linear regime.

The parameter a already introduced in Section 1, is defined as the ratio between a^*, which is the amplitude of the initial edge wave, and the undisturbed water depth h_0^* both evaluated at $x = 0$. For small values of a (a less than about 10^{-3}) only the harmonics characterized by $n = \pm 1$ in (11) attain significant values, even if longshore averaged and second harmonic components ($n = 0, \pm 2$) are found but with an amplitude which is many orders of magnitude smaller than that characterizing the basic harmonic component ($n = \pm 1$). Fig. 4, where the free surface elevation at a fixed position near the shore is plotted versus time for a equal to 1.8×10^{-3}, shows that, as expected, the free surface experiences periodic oscillations of period 2π.

Even if nonlinear effects are so weak as to be considered negligible from a practical point of view, they are present and are reproduced by the numerical solution. Indeed an aspect of nonlinearity, which can be easily guessed on the basis of theoretical considerations and it is reproduced by the numerical solution, is the presence of a two-dimensional wave which travels in the offshore direction [3] and drains energy from the coastal region. As a consequence, the energy of the waves trapped close to

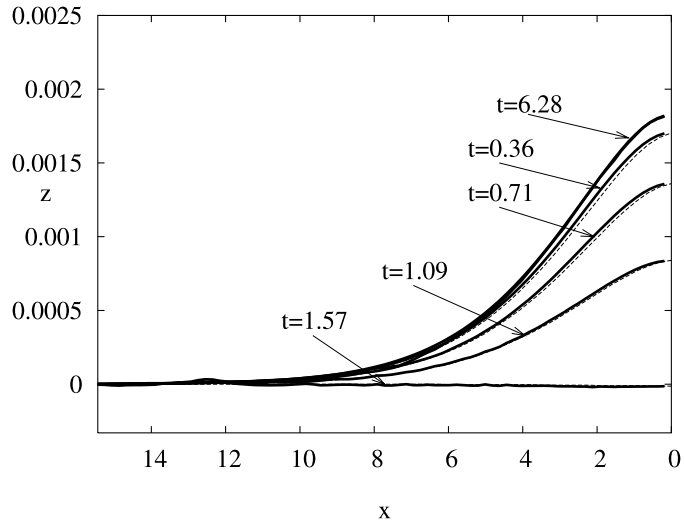

Fig. 5. Time evolution of a free surface perturbation initially periodic in the longshore direction and characterized by $L_y = 6.97$, $a = 1.7 \times 10^{-3}$ ($x_w = 11.58$). In the figure both the numerical and the analytical results of the linearized problem are shown at different times (— numerical solution, - - - analytical solution).

the coast decreases and the amplitude of the edge wave becomes smaller. Indeed a closer inspection of Fig. 4 shows a small decay of the edge wave amplitude which is related to a small leak of energy related to the presence of the 2-D wave, which propagates toward the deep water region. Tests have been made to ascertain that the amplitude decay shown in Fig. 4 is a physical phenomenon and not a numerical effect. Indeed the results shown in Fig. 4 are independent on the grid size and time step. A quantitative comparison between the theoretical solution by Blondeaux et al. [18] and the present numerical results is shown in Fig. 5, where the cross-shore structure of the edge wave profile at the antinode located at $z = 0$ is plotted at different phases of the cycle. The comparison shows that (9) provides a good description of the solution for very small values of a.

As a is increased, nonlinear effects become more relevant and the functions used to build up the initial conditions do not satisfy the equations. Therefore an initial transient has been discarded in the analysis of the results.

3.1. Weakly nonlinear regime

For moderate values of the parameter a, more harmonic components are generated due to nonlinear effects. The presence of harmonic components of smaller wavelength is apparent looking at the results of a run carried out with $a = 0.017$, a value which is one order of magnitude larger than that characteristic of the linear regime.

The time evolution of the first three longshore harmonic components defined by (11) is shown in Fig. 6. It can be observed that the amplitude of the first harmonic does not appear to decay significantly. Indeed the amplitude of the outgoing wave is still very small. Nevertheless nonlinear effects are not negligible and nonlinearity causes the appearance of significant higher harmonics in the flow field. Moreover a peculiar time evolution of the amplitude of the first two ultraharmonic components is observed. Indeed after an initial transient, a modulation of their amplitude appears. The modulation is the result of a resonant interaction between different edge wave modes. Indeed, in the following, it is shown that the modulation of the first two components can be predicted also on the basis of a weakly nonlinear analysis.

The solution of the governing equations (2) in the weakly nonlinear regime can be expressed by the following perturbation expansion based on the small parameter a:

$$(\eta, u, v) = a(\eta_0, u_0, v_0) + a^2(\eta_1, u_1, v_1) + \mathrm{O}(a^3), \tag{12}$$

where the symbol 'O' denotes order of magnitude. By substituting (12) into (2), a sequence of problems is obtained which determine the flow field at the different orders of approximation. At O(a) the linearized problem is found:

$$\frac{\partial \eta_0}{\partial t} + \frac{\partial [u_0 h]}{\partial x} + \frac{\partial [v_0 h]}{\partial y} = 0,$$

$$\frac{\partial u_0}{\partial t} + \frac{\partial \eta_0}{\partial x} = 0,$$

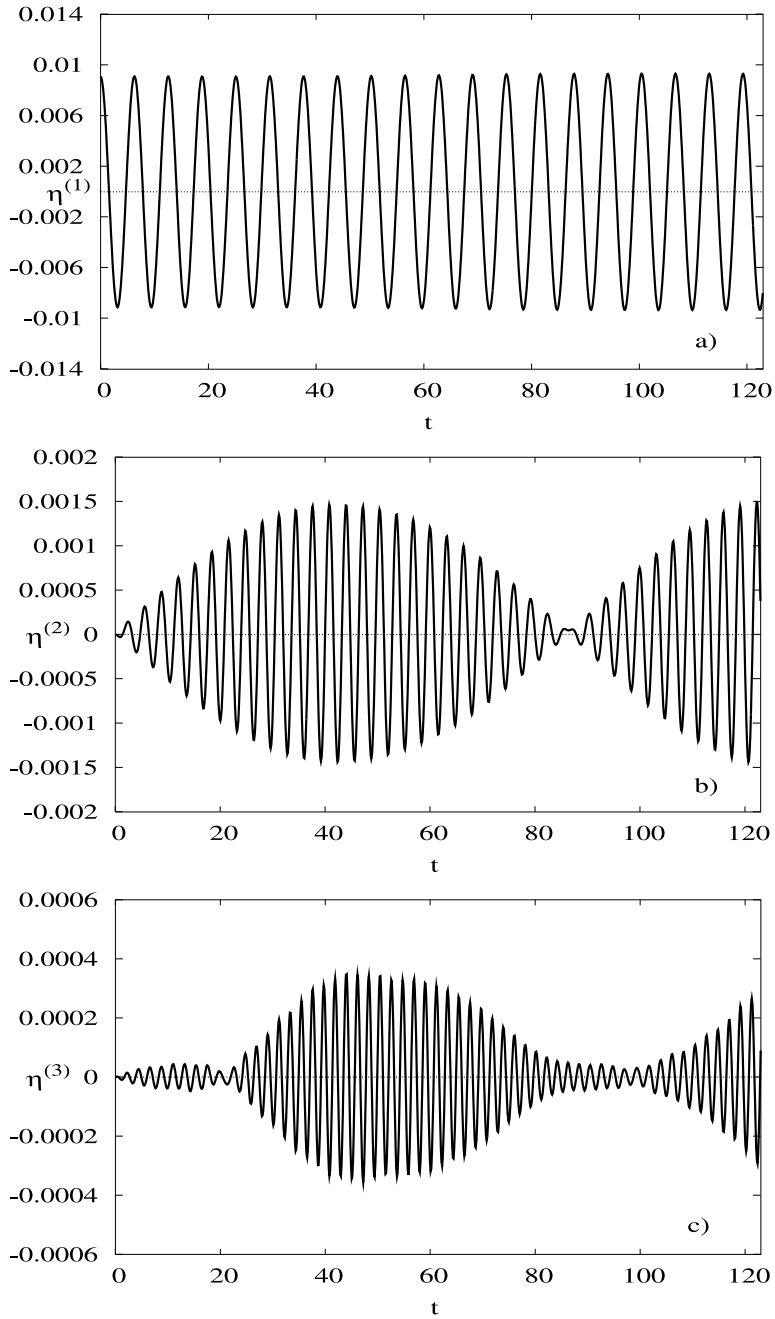

Fig. 6. $\eta^{(n)}$ at $x = 0$ versus time for an initial perturbation periodic in the longshore direction characterized by $L_y = 6.97$, $a = 0.017$ ($x_w = 11.58$); (a) $\eta^{(1)}$, (b) $\eta^{(2)}$, (c) $\eta^{(3)}$.

$$\frac{\partial v_0}{\partial t} + \frac{\partial \eta_0}{\partial y} = 0. \tag{13}$$

The solution of which is provided by (9). Let us consider the time evolution of an initial surface elevation obtained by the superposition of four different edge wave modes:

$$\begin{aligned}\eta_0(x,z,t,\tau) = {} & A_1(\tau)\hat{\eta}_{01}(x)\exp\big[i(k_1 z + t)\big] + A_1(\tau)\hat{\eta}_{01}(x)\exp\big[i(k_1 z - t)\big] \\ & + A_2(\tau)\hat{\eta}_{02}(x)\exp\big[i(k_2 z + \omega_2 t)\big] + A_2(\tau)\hat{\eta}_{02}(x)\exp\big[i(k_2 z - \omega_2 t)\big] + \text{c.c.}\end{aligned} \tag{14}$$

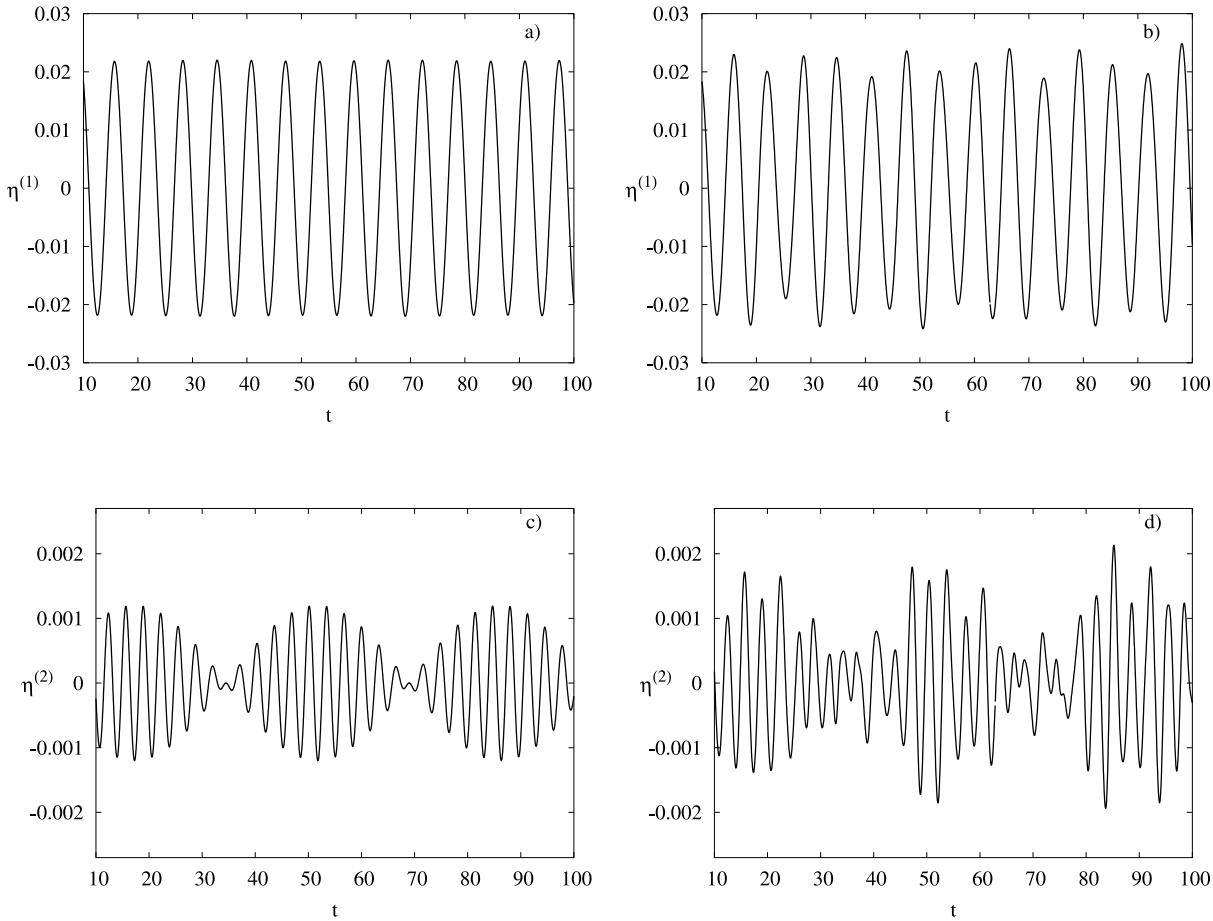

Fig. 7. First ($\eta^{(1)}$) and second ($\eta^{(2)}$) edge wave components at $x = 0$ versus time for $x_w = 3$ and an initial perturbation characterized by $a_0 = 0.044$, $k_1 = 0.7633$. Results of the model equation (18) (a), (c) and numerical simulations of the full shallow water equations (2) (b), (d).

where c.c. denotes complex conjugate and $\tau = at$ is a slow time scale characteristic of the growth of the edge waves amplitudes. The first component is the fundamental edge wave mode with a period equal to 2π and wavenumber obtained by (10). The second component describes an edge wave with the same characteristics as those of the first one, but traveling in the opposite direction. We assume that the wavenumber of the third and fourth components is related to that of the first one by:

$$k_2 = 2k_1. \tag{15}$$

The dispersion relationship (10) gives the value of the angular frequency σ_2. It can be easily checked that it is feasible to assume

$$\omega_2 = 2 + a\mu, \tag{16}$$

where μ is a detuning parameter. The problem at order $O(a^2)$ turns out to be:

$$\begin{aligned}
&\frac{\partial \eta_1}{\partial t} + \frac{\partial [hu_1]}{\partial x} + \frac{\partial [hv_1]}{\partial y} = -\frac{\partial [u_0\eta_0]}{\partial x} - \frac{\partial [v_0\eta_0]}{\partial y} - \frac{\partial \eta_0}{\partial \tau},\\
&\frac{\partial u_1}{\partial t} + \frac{\partial \eta_1}{\partial x} = -u_0\frac{\partial u_0}{\partial x} - v_0\frac{\partial u_0}{\partial y} - \frac{\partial u_0}{\partial \tau},\\
&\frac{\partial v_1}{\partial t} + \frac{\partial \eta_1}{\partial y} = -u_0\frac{\partial v_0}{\partial x} - v_0\frac{\partial v_0}{\partial y} - \frac{\partial v_0}{\partial \tau}.
\end{aligned} \tag{17}$$

The homogeneous part of (17) is the same as (13) and admits a non-trivial solution. Moreover the forcing terms in the right-hand side of (17) reproduce the spatial and temporal structure of the solution of the homogeneous problem because of (15) and (16). Hence, to avoid a secular growth of the solution, it is necessary to force a solvability condition (described

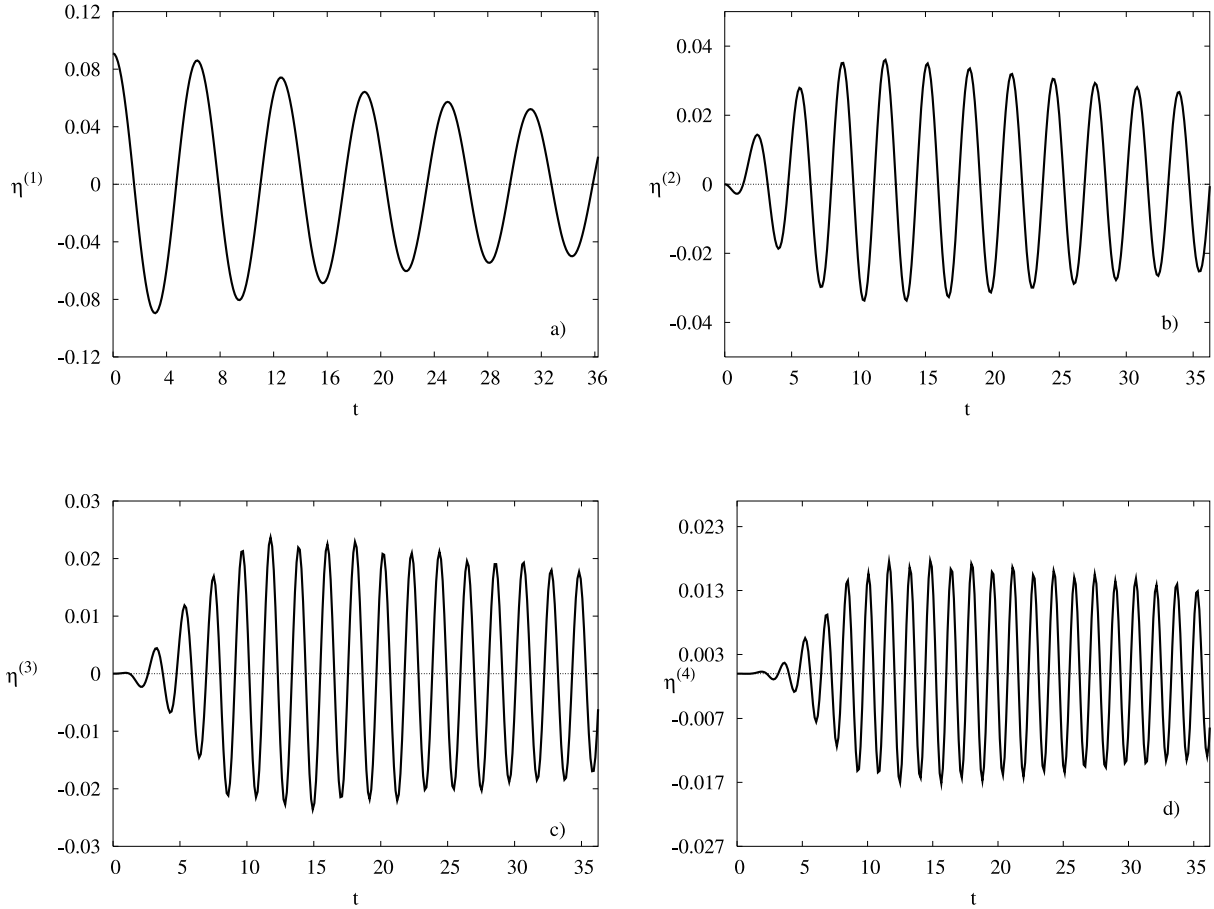

Fig. 8. $\eta^{(n)}$ at $x = 0$ versus time for an initial perturbation periodic in the longshore direction characterized by $L_y = 6.97$, $a_0 = 0.17$; (a) $\eta^{(1)}$, (b) $\eta^{(2)}$, (c) $\eta^{(3)}$, (d) $\eta^{(4)}$.

more extensively in the Appendix) which leads to a system of differential equations describing the time evolution of $A_1(\tau)$ and $A_2(\tau)$:

$$a_0 \frac{\mathrm{d}A_1}{\mathrm{d}\tau} + a_1 A_2 \overline{A_1}\, \mathrm{e}^{\mathrm{i}\mu\tau} = 0,$$
$$b_0 \frac{\mathrm{d}A_2}{\mathrm{d}\tau} + b_1 A_1^2\, \mathrm{e}^{-\mathrm{i}\mu\tau} = 0. \tag{18}$$

In (18) an overbar denotes the complex conjugate of a complex quantity.

The form of the coefficients a_0, b_0, a_1 and b_1, which depend on the beach parameter x_w, is given in the Appendix. The system of ordinary differential equations (18) is presently solved numerically by means of a Runge–Kutta approach of the second order.

Fig. 7 shows the typical time evolution of A_1 and A_2 obtained by both the integration of (18) and by the numerical simulation of the full shallow water equations (2). The agreement between the theoretical and numerical results is fair. Indeed the modulation of the second harmonic component, obtained by means of the theoretical analysis, takes place with the same period as that of the numerical simulations and with similar amplitudes. Moreover, the amplitude of the first harmonic component keeps almost constant, even though the numerical solution is characterized by small oscillations which appear to be random. These oscillations are due to the presence of many harmonic components which are generated in the fully nonlinear solution and interact in a complex way. A theoretical investigation of the nonlinear interaction of different edge wave components similar to that developed in the present paper has been proposed by Blondeaux and Vittori [27] for a constant sloping beach. They showed that the different longshore components exchange energy with each other on a time scale which is much longer than the edge wave period and modulations of $\eta^{(2)}$ and $\eta^{(3)}$ are expected to take place forced by an incoming wave. However in Blondeaux

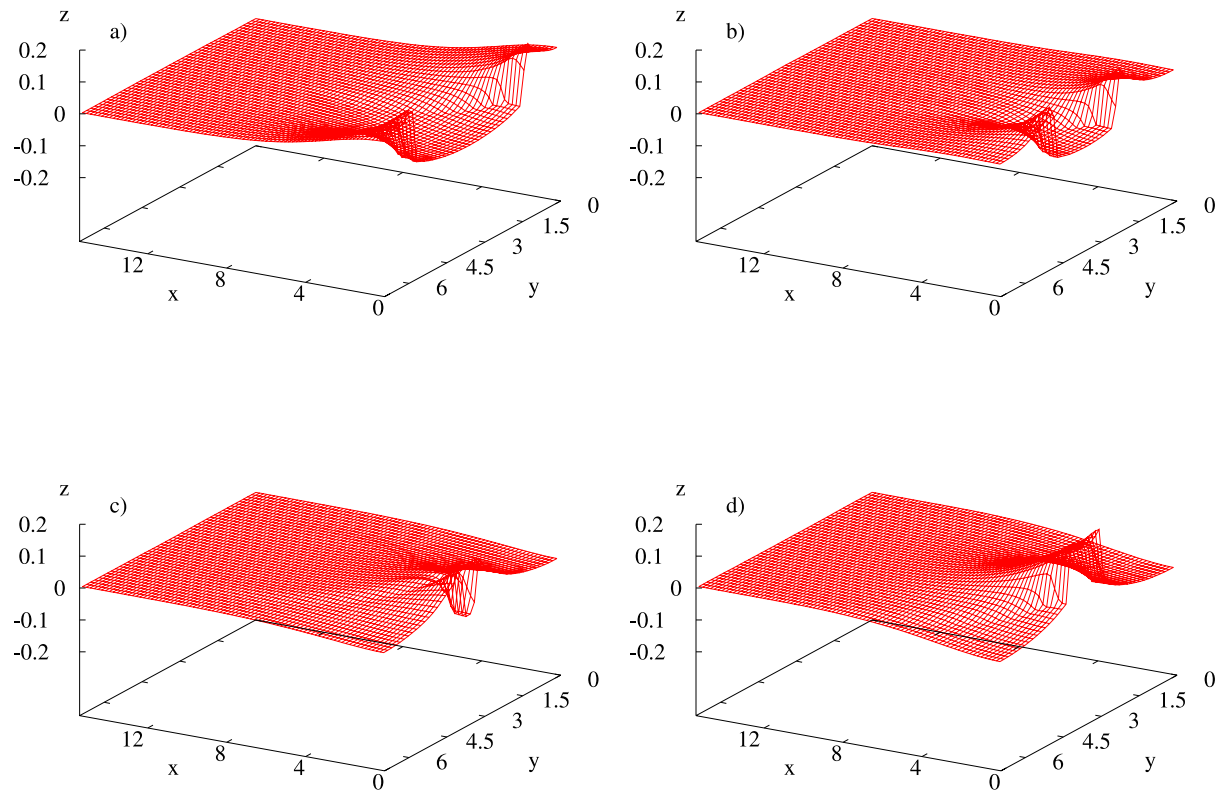

Fig. 9. Time evolution of a free surface perturbation initially periodic in the longshore direction and characterized by $L_y = 6.97$, $a = 1.7 \times 10^{-1}$ ($x_w = 11.58$): (a) $t = 31.42$, (b) $t = 32.27$, (c) $t = 33.12$, (d) $t = 33.97$.

and Vittori [27] the amplitude of the different harmonics grows because the wave which approaches the coastline from the deep water region provides an energy input to the whole system.

It has been possible to integrate the system (18) numerically only for beaches characterized by moderate values of x_w due to the difficulties encountered to compute the Kummer function U appearing in (9) when x_w assumes large values. A series of runs performed varying the non-dimensional parameters and the initial conditions has shown that the frequency of the modulation of the amplitude of A_1 and A_2 is linearly related to the detuning parameter μ. As the parameter x_w is increased, the period of the modulation of both A_1 and A_2 and the amplitude of the modulation of the second component increases while that of A_1 does not show a distinct tendency.

3.2. *Fully nonlinear regime*

The resonance phenomenon previously described disappears as a is increased, since for larger values of a many harmonics are generated by nonlinear effects and interact in a complex way. An example of the results obtained for $a = 0.17$ is shown in Fig. 8, where the values of $\eta^{(n)}$ are plotted versus time for n =1, 2, 3 and 4. From the results plotted in Fig. 8, it can be appreciated that the decay in time of the first component $\eta^{(1)}$ takes place quite rapidly. This decay can be partly ascribed to the generation of a two-dimensional outgoing wave which causes the radiation of energy toward the deep water region to become significant (see Fig. 13). A further mechanism which can cause a drain of the edge wave energy is the formation of a steep front (bore) which induces energy dissipation. Fig. 8 shows that after 5 periods, the amplitude of the first component of the edge wave is reduced of approximately 40%. Hence, edge waves of large amplitude cannot survive without a continuous supply of energy. As clearly discussed in the book of Mei [3], edge waves of constant amplitude can exist only when a 2-D wave, approaching the coastline from the deep water region, transfers energy to them. Ultraharmonic components $\eta^{(n)}$ ($n > 1$), after an initial transient, slowly decay because the energy of the whole system decreases. It has been observed that at the end of the simulation ($t = 5T$), $\eta^{(2)}$ attains a value which is approximately 30% of the initial amplitude of the disturbance. The harmonic components with smaller longshore wavelength have amplitudes of the same order of magnitude (the 6th component attains a value which is approximately 10% of the amplitude of initial disturbance) thus indicating the relevance of nonlinear effects.

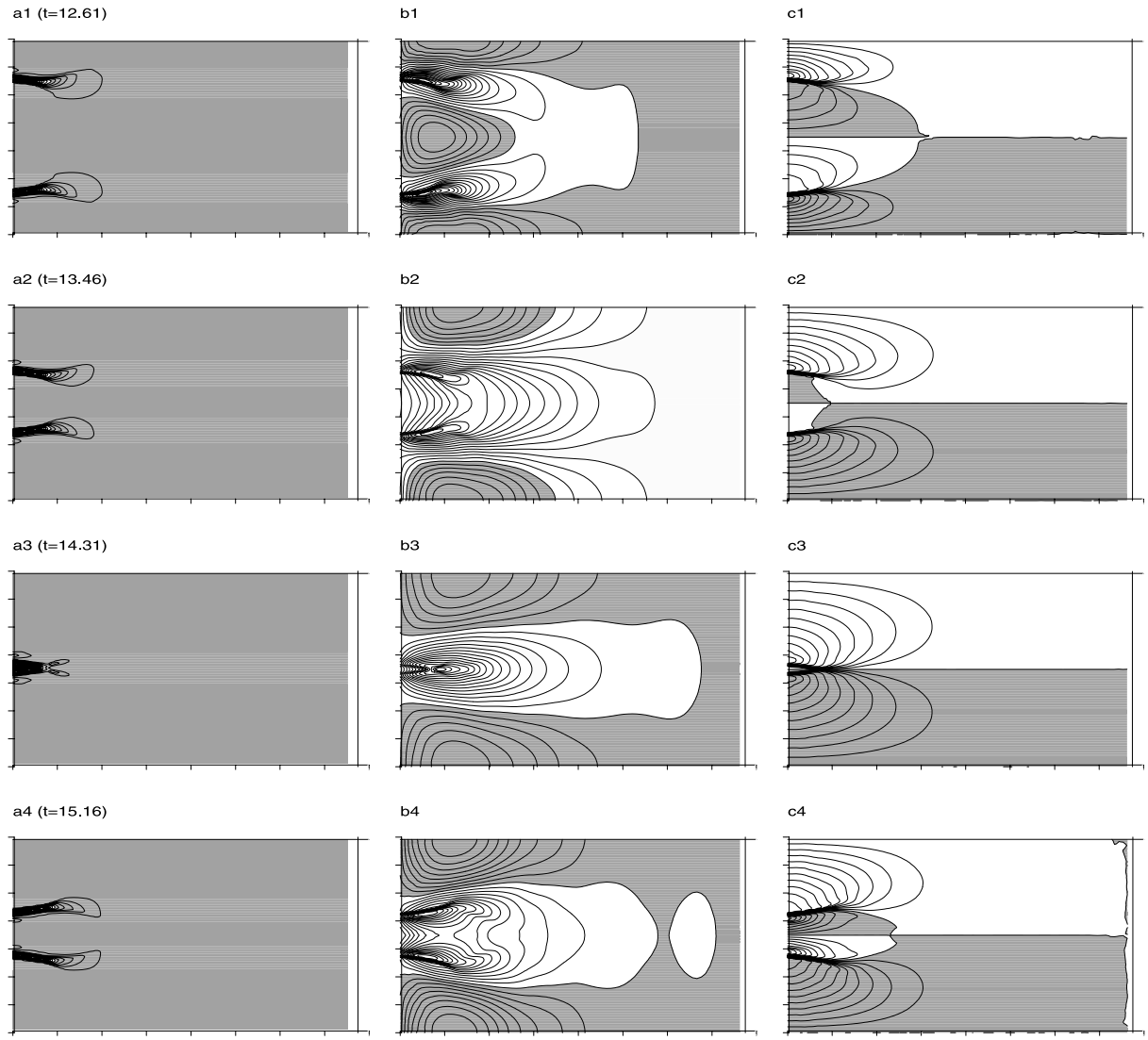

Fig. 10. Time evolution of a free surface perturbation characterized by $L_y = 6.97$, $a_0 = 1.7 \times 10^{-1}$ ($x_w = 11.58$). First column, free surface gradient; second column, cross-shore velocity; third column, long-shore velocity. A cross-shore extent equal to 15.44 is displayed in the horizontal axis while the longshore extent is equal to 6.97 and displayed in the vertical axis. Shaded regions are characterized by positive values. (a1) max = 8.203, min = 0.432, $\Delta = 0.389$; (a2) max = 8.203, min = 0.432, $\Delta = 0.389$; (a3) max = 8.203, min = 0.432, $\Delta = 0.389$; (a4) max = 8.203, min = 0.432, $\Delta = 0.389$; (b1) max = 0.018, min = -0.006, $\Delta = 0.001$; (b2) max = 0.024, min = -0.017, $\Delta = 0.002$; (b3) max = 0.052, min = -0.019, $\Delta = 0.004$; (b4) max = 0.022, min = -0.013, $\Delta = 0.002$; (c1) max = 0.129, min = -0.129, $\Delta = 0.011$; (c2) max = 0.184, min = -0.184, $\Delta = 0.017$; (c3) max = 0.221, min = -0.221, $\Delta = 0.020$; (c4) max = 0.100, min = -0.100, $\Delta = 0.009$.

The relevance of nonlinear effects is also revealed by the inspection of the longshore edge wave profile which is no longer symmetric with respect to the mean water level. In particular, each of the two edge waves, propagating in opposite directions and giving rise to the steady edge wave, shows a front slope steeper than the rear one. As a consequence the presence of the two components propagating in opposite directions becomes evident and large surface gradients are observed close to their crests as clearly shown by Fig. 9. The propagating crests cause the formation of jets in the cross-shore direction as can be appreciated by looking at Fig. 10. The velocity field associated with the propagating crests shows the presence of regions of strong negative cross-shore velocity close to the wave fronts (see the second column of Fig. 10). These regions follow the fronts and, hence, propagate in opposite longshore directions. When the two fronts reach the center of the domain and meet, a shore-ward jet of water is generated (see Fig. 10, b3). In the third column of Fig. 10 the longshore velocity is plotted. The v component of velocity is positive behind the crest propagating in the positive direction and vice versa, to balance the mass

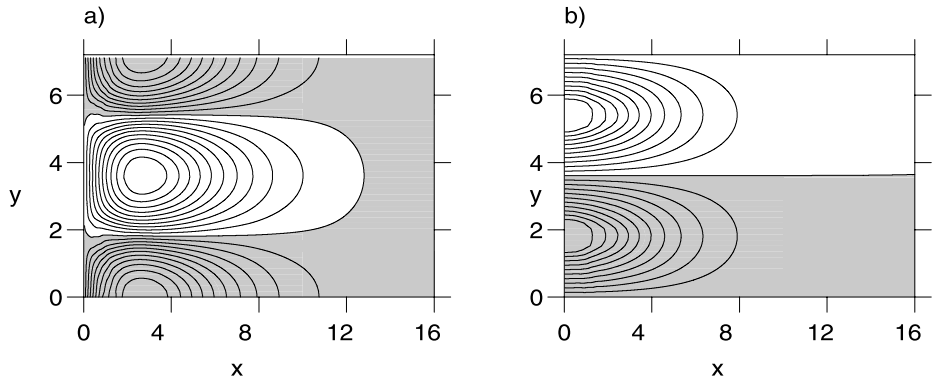

Fig. 11. Velocity components averaged between $t = 2T$ and $t = 2T + T/2$. The initial perturbation is periodic in the longshore direction and characterized by $L_y = 6.97$, $a_0 = 1.7 \times 10^{-1}$ ($x_w = 11.58$). (a) Cross-shore velocity component (max $= 0.0147$, min $= -0.0147$, $\Delta = 0.0015$, (b) longshore velocity component (max $= 0.083$, min $= -0.083$, $\Delta = 0.04083$). Shaded regions are characterized by positive values.

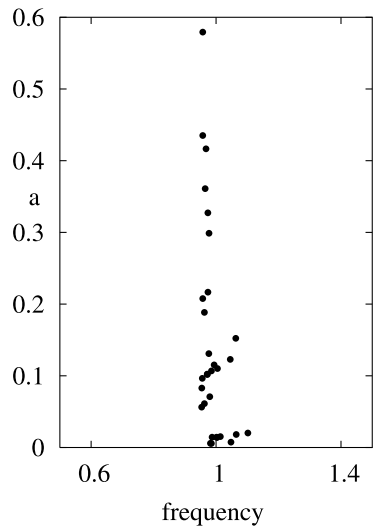

Fig. 12. Dimensionless edge waves frequency versus a for an initial perturbation characterized by $L_y = 6.97$ ($x_w = 11.58$).

flux associated to the propagation of the crests. Fig. 10 shows the time evolution of the solution during half edge wave cycle; the same pattern is repeated during the following half of the cycle but shifted in the longshore direction of half the edge wave length. Therefore shore-ward currents appear every $T/2$ alternatively at $y = L_y/2, 3L_y/2, 5L_y/2, \ldots$, and $y = 0, L_y, 2L_y, \ldots$. A similar conclusion is obtained by considering the time averaged velocity field. Fig. 11 shows the long-shore and cross-shore velocity components averaged from $t = 2T$ to $t = 2T + T/2$ for values of the parameters equal to those leading to the results shown in Fig. 10. The results show that the averaged fluid motion is characterized by a shore-ward current in the middle of the computational box and by sea-ward currents along the sides. The longshore velocity component is directed from the sides to the center of the fluid domain. Qualitatively similar results are obtained performing the time average during the following half cycle from $t = 2T + T/2$ to $t = 3T$. However, the flow pattern is shifted of $L_y/2$ in the longshore direction and shore-ward directed currents are present at the sides of the flow domain while the steady cross-shore velocity component is directed off-shore in the center of the computational box. Moreover due to the radiation of energy in the off-shore direction, the edge wave decay and the currents during the following half cycle are weaker.

Another interesting finding which comes from the analysis of the results for moderate and large values of the parameter a is the dependence of the free mode frequency on the edge wave amplitude. For a constant sloping beach, without the vertical wall, it is known that in the weakly nonlinear regime the linear dispersion relationship is modified by the presence of a term proportional to the square of the edge wave amplitude [21]. Fig. 12 shows the frequency for the model beach (1) versus a, obtained by means of the numerical simulations. Surprisingly it can be seen that, even for large values of a such that nonlinear effects are found to be relevant and generate the presence of many harmonic components, the edge waves period is almost

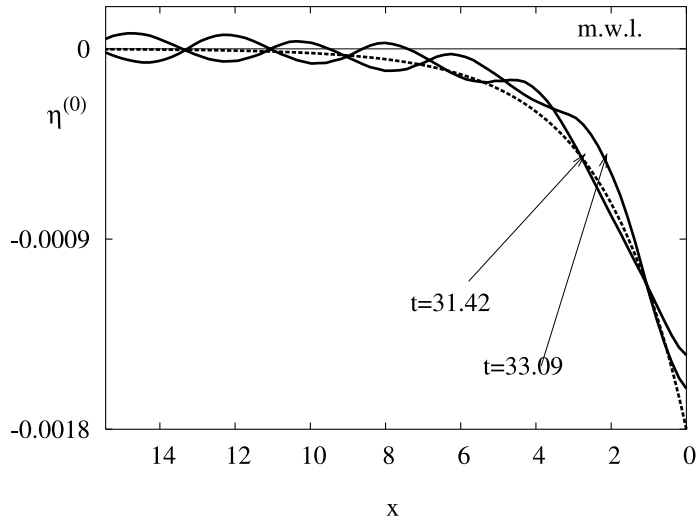

Fig. 13. Free surface elevation averaged in the long-shore direction versus the cross shore coordinate at two different phases, for an initial perturbation characterized by $a_0 = 0.17$. ($L_y = 6.97, x_w = 11.58$) $---$ Set-down induced by free edge waves on a constant sloping beach according to the analysis by Guza and Bowen [21] (edge wave wavelength equal to that of the numerical computations).

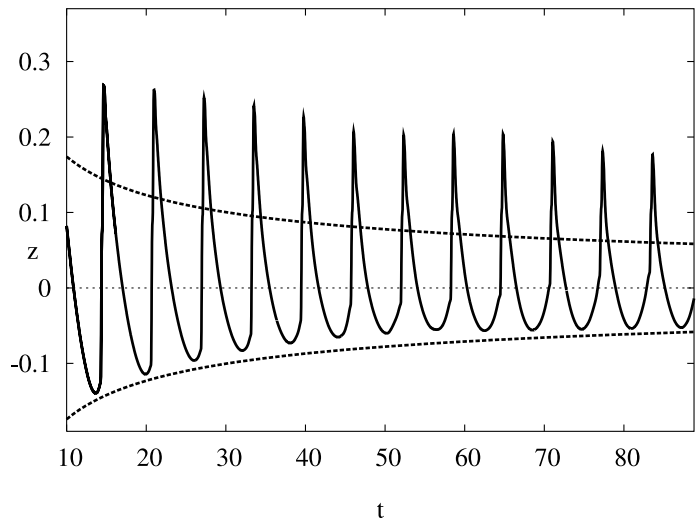

Fig. 14. Time evolution of the free surface displacement at $x = 0.31$ and $y = 3.49$ for an initial perturbation characterized by $a_0 = 0.17$ ($L_y = 6.97$, $x_w = 11.58$) (solid line).
Envelope of the amplitude of the edge wave at the same location for a constant sloping beach without the vertical wall ($L_y = 6.97$, $\beta = 10^{-2}$) according to the analytical solution by [21] (broken line).

independent on a. Therefore it appears that even though the dynamics of the edge waves in the weakly and fully nonlinear regimes is markedly different from that of the linear regime, the dispersion relationship appears to be practically unaffected. For very small values of a, the evaluation of the frequency becomes inaccurate with the number of grid points presently used. This is the cause of the scatter of the frequency which is observed in Fig. 12 as a tends to vanish.

Nonlinear effects are also known to generate a set-down close to the beach. Surprisingly, a comparison between the present results and those derived by the weakly nonlinear analytical analysis by Guza and Bowen [21] performed for a constant sloping beach (Eckart's profile) characterized by the same value of β but without the vertical wall, has shown that the set-down on the two beaches is similar (see Fig. 13) notwithstanding the different beach geometry and the large nonlinear effects. Also the wave damping is similar (see Fig. 14). Indeed in the weakly nonlinear regime for a constant sloping beach without vertical

wall, it is known [21], that the rate of decay of edge wave amplitude is proportional to $t^{-0.5}$. Presently the presence of strong nonlinear effects, which causes sharp peaks in the time evolution of surface elevation at a particular location, makes the visual estimation of the decay difficult. However the trend of the wave amplitude envelope appears similar to that predicted by Guza and Bowen [21] (see Fig. 14).

4. Conclusions

The shallow water equations are solved numerically by means of the WAF method on a model beach suitable to describe large scale motions in the region offshore of the breakers' line. Attention is focused on the free edge wave modes with periods of the order of minutes or longer. The aim of the paper is to determine when nonlinear effects become relevant and to investigate when the interaction among different harmonic components may lead to complex wavefield and to the generation of steady current patterns difficult to predict by analytical means. A comparison between numerical findings and linear and weakly nonlinear analytical solutions is presented.

Three regimes have been identified depending on the value of the nonlinearity parameter a which is equal to the ratio between the edge wave amplitude and the water depth at the position $x = 0$. In the linear regime, observed for very small values of a, nonlinear effects are very weak and can thus be neglected. For moderate values of a, nonlinear effects cause the generation of significant higher harmonic components and they induce a resonance phenomenon between the different components which causes a modulation in time of their amplitude. In the fully nonlinear regime, observed for large values of a, many harmonic components are present which interact in a complex way. Moreover, intermittent currents directed in the cross-shore direction have been observed.

For convenience, the results are presented and discussed in dimensionless form. To give an idea of the practical relevance of the present computations, let us consider dimensional quantities. For an edge wave of period equal to 2 minutes on a model beach (1) characterized by h_0^* equal to about 2 meters and $\beta = 2 \times 10^{-3}$, on the basis of the present results, it can be stated that the linear regime applies to edge waves characterized by amplitudes of the order of 10^{-3} meters, the weakly nonlinear regime to edge waves of amplitude of few centimeters while the solution of the full problem should be considered when the edge wave amplitude becomes larger than 10 centimeters.

As discussed in the introduction, edge wave amplitudes of the order of 10^{-1} m might appear to be unrealistic, since field measurements (see a.o. Oltman-Shay and Guza [19]) seem to suggest values of order 10^{-2} m. However, it should be considered that field measurements are usually carried out for mild wave climate and in open coasts. Edge waves generated by more severe wave climate and in particular during storms are expected to be significantly larger. Moreover in pocket beaches, resonance phenomena can induce even larger edge wave amplitudes.

The qualitative differences observed between the linear, weakly nonlinear and fully nonlinear regimes suggest that caution must be used to apply the results obtained by means of linear and weakly nonlinear analytical approaches to describe field cases characterized by large amplitudes, since nonlinear effects might be relevant and some aspects of the phenomenon might not be captured.

Appendix

At $O(a^2)$, the governing equations (17) can be combined to obtain a single equation for η_1:

$$\frac{\partial^2 \eta_1}{\partial t^2} - \frac{\partial}{\partial x}\left[h\frac{\partial \eta_1}{\partial x}\right] - \frac{\partial}{\partial y}\left[h\frac{\partial \eta_1}{\partial y}\right] = \mathcal{F}, \tag{A1}$$

where

$$\begin{aligned}\mathcal{F} = {} & -2\frac{\partial \eta_0}{\partial t\,\partial \tau} + \frac{1}{x_w}\left[u_0\frac{\partial u_0}{\partial x} + v_0\frac{\partial u_0}{\partial y}\right] + h\left[\left(\frac{\partial u_0}{\partial x}\right)^2 + u_0\frac{\partial^2 u_0}{\partial x^2} + \frac{\partial v_0}{\partial x}\frac{\partial u_0}{\partial y} + v_0\frac{\partial^2 u_0}{\partial x\,\partial y} + \frac{\partial u_0}{\partial y}\frac{\partial v_0}{\partial x} + u_0\frac{\partial^2 v_0}{\partial x\,\partial y}\right. \\ & \left. + \left(\frac{\partial v_0}{\partial y}\right)^2 + v_0\frac{\partial^2 v_0}{\partial y^2}\right] - \frac{\partial}{\partial t\,\partial x}(u_0\eta_0) - \frac{\partial}{\partial t\,\partial y}(v_0\eta_0).\end{aligned} \tag{A2}$$

After substituting the solution η_0, u_0 and v_0 of the problem at the previous order of approximation, $\mathcal{F}$ can be expressed in the form:

$$\mathcal{F} = \left[f_1(x)\frac{\mathrm{d}A_1}{\mathrm{d}\tau} + f_2(x)\,\mathrm{e}^{\mathrm{i}\mu\tau}A_2\overline{A}_1\right]\mathrm{e}^{\mathrm{i}(k_1 y + t)} + \left[g_1(x)\frac{\mathrm{d}A_2}{\mathrm{d}\tau} + g_2(x)\,\mathrm{e}^{-\mathrm{i}\mu\tau}A_1^2\right]\mathrm{e}^{\mathrm{i}(k_2 y + \omega_2 t)} + \cdots, \tag{A3}$$

where f_1, f_2, g_1 and g_2 are long expressions which can be easily worked out and are not given here for the sake of brevity. The terms not explicitly indicated in (A3) are not relevant to write the solvability condition. Since the homogeneous part of Eq. (A1) admits a nontrivial solution, Eq. (A1) has a bounded solution if and only if a solvability condition is enforced which leads to

$$a_0 \frac{\mathrm{d}A_1}{\mathrm{d}\tau} + a_1 \mathrm{e}^{\mathrm{i}\mu\tau} A_2 \overline{A}_1 = 0,$$
$$b_0 \frac{\mathrm{d}A_1}{\mathrm{d}\tau} + b_1 \mathrm{e}^{-\mathrm{i}\mu\tau} A_1^2 = 0, \tag{A4}$$

where

$$a_0 = \int_{x_w}^{\infty} f_1(x)\hat{\eta}_{01}(x)\,\mathrm{d}x, \qquad a_1 = \int_{x_w}^{\infty} f_2(x)\hat{\eta}_{01}(x)\,\mathrm{d}x,$$
$$b_0 = \int_{x_w}^{\infty} g_1(x)\hat{\eta}_{02}(x)\,\mathrm{d}x, \qquad b_1 = \int_{x_w}^{\infty} g_2(x)\hat{\eta}_{02}(x)\,\mathrm{d}x. \tag{A5}$$

References

[1] D. Huntley, Long period waves on a natural beach, J. Geoph. Res. 81 (36) (1976) 6441.
[2] R.A. Holman, A.J. Bowen, Edge waves on complex beach profiles, J. Geoph. Res. 84 (C10) (1979) 6339.
[3] C.C. Mei, The Applied Dynamics of Ocean Surface Waves, World Scientific, 1989.
[4] R.T. Guza, R.E. Davis, Excitation of edge waves by waves incident on a beach, J. Geoph. Res. 79 (1974) 1285.
[5] R.T. Guza, A.J. Bowen, Finite amplitude edge waves, J. Mar. Res. 34 (1976) 269–293.
[6] A.A. Minzoni, G.B. Whitham, On the excitation of edge waves, J. Fluid Mech. 79 (1977) 273.
[7] P.H. LeBlond, L.A. Mysak, Waves in the Ocean, Elsevier, 1978.
[8] A.J. Bowen, Rip currents 1: theory, J. Geoph. Res. 74 (1969) 5467.
[9] A.J. Bowen, D.L. Inman, Rip currents, 2, Laboratory and field observations, J. Geoph. Res. 74 (23) (1969) 5479.
[10] D.L. Inman, R.T. Guza, The origin of swash cusps on beaches, Marine Geology 49 (1982) 133.
[11] R.A. Holman, A.J. Bowen, Bars, bumps, and holes: models for the generation of complex beach topography, J. Geoph. Res. 87 (C1) (1982) 457.
[12] P.A. Howd, A.J. Bowen, R.A. Holman, Edge waves in the presence of strong longshore currents, J. Geoph. Res. 97 (C7) (1992) 11–357.
[13] H.J. Schonfeldt, On the modification of edge waves by longshore currents, Cont. Shelf. Res. 15 (1995) 1213.
[14] K.R. Bryan, A.J. Bowen, Edge wave trapping and amplification on barred beaches, J. Geoph. Res. 101 (C3) (1996) 6543.
[15] G. Vittori, H. De Swart, P. Blondeaux, Crescentic bedforms in the nearshore region, J. Fluid Mech. 381 (1999) 271.
[16] C. Eckart, Surface waves on water of variable depth, Wave Rep. 100 Scripps Inst. of Oceanogr. Univ. of California, La Jolla, 1951.
[17] F.K. Ball, Edge waves in an ocean of finite depth, Deep-Sea Res. 14 (1967) 79.
[18] P. Blondeaux, G. Vittori, H. De Swart, Subharmonic edge wave excitation by waves incident on partially absorbing beaches, in: Proceedings EUROMECH 310, World Scientific, 1994.
[19] J. Oltman-Shay, R.T. Guza, Infragravity edge wave observations on two California beaches, J. Phys. Oceanogr. 17 (1987) 644.
[20] H.T. Őzkan-Haller, C. Vidal, I.J. Losada, R. Medina, M. Losada, Standing edge waves on a pocked beach, J. Geoph. Res. 106 (C8) (2001).
[21] R.T. Guza, A.J. Bowen, Resonant interactions for waves breaking on a beach, in: Proc. 15th Int. Conf. of Coast. Engrg., vol. 1, 1976, p. 560.
[22] F.I. Gonzales, K. Satake, E.F. Boss, H.O. Mofjeld, Edge waves and non-trapped modes of the 25 April 1992 Cape Mendocino Tsunami, Pure Appl. Geoph. 144 (3/4) (1995).
[23] E.F. Toro, Riemann problems and the WAF method for solving the two-dimensional shallow water equations, Phil. Trans. R. Soc. London 338 (1992) 43.
[24] G. Watson, D.H. Peregrine, Low frequency waves in the surf zone, in: Proc. 23th Int. Conf. Coast. Engrg., vol. 1, 1992, p. 818.
[25] M. Brocchini, G. Vittori Report on an efficient solver for the nonlinear shallow water equations able to deal with steady currents and mode–mode interaction. Task M2.6.1 Report, HUMOR Project, Genova Workshop, 2001.
[26] M. Brocchini, R. Bernetti, A. Mancinelli, G. Albertini, An efficient solver for nearshore flows based on the WAF method, Coast. Engrg. 43 (2) (2001) 105–129.
[27] P. Blondeaux, G. Vittori, The nonlinear excitation of synchronous edge waves by a monochromatic wave normally approaching a plane beach, J. Fluid Mech. 301 (1995) 251.
[28] J.T. Kirby, U. Putrevu, H.T. Őzkan-Haller, Evolution equations for edge waves and shear waves on longshore uniform beaches, in: Proc. 26th Int. Conf. Costal Engrg., 1998, pp. 203–216.
[29] K.E. Kenyon, A note on conservative edge waves interaction, Deep-Sea Res. 17, 197-201.

[30] P.A. Howd, W.A. Birkemeijer, Beach and nearshore survey data: 1981–1984 CERC Field Research Facility, Tech. Report CERC 87-9 Coastal Engrg. Res. Center, USAE Waterways Experiment Station, Vicksburg, MS.
[31] G. Lee, W.A. Birkemeijer, Beach and nearshore survey data: 1985–1991 CERC Field Research Facility, Tech. Report CERC 93-3 Coastal Engrg. Res. Center, USAE Waterways Experiment Station, Vicksburg, MS.
[32] M. Hom-ma, C. Sonu, Rhythmic pattern of longshore bars related to sediment characteristics, in: Proceedings of the 8th Coastal Engineering Conference, 1963, pp. 248–278.
[33] Z. Pruszak, G. Rozynsky, R.B. Zeidler, Statistical properties of multiple bars, Coastal Engrg. 31 (1997) 263–280.
[34] V. Galletta, Studio numerico-sperimentale dell'idrodinamica costiera, Ph.D. Thesis, Dipartimento di Ingegneria Ambientale, Genova, 2000.
[35] E.F. Toro, Riemann Solvers and Numerical Methods for Fluid Dynamics, Springer, 1997.
[36] G. Watson, D.H. Peregrine, E.F. Toro, Numerical solutions of the shallow water equations on a beach using the Weighted Averaged Flux method, in: Computational Fluid Dynamics '92, vol. 1, Elsevier, 1992.
[37] E.F. Toro, Shock-Capturing Methods for Free-Surface Shallow Flows, Wiley, 2001.
[38] M. Abramovitz, I. Stegun, Handbook of Mathematical Functions, Dover, New York, 1965.